The Aleutian Low and Winter Climatic Conditions in the Bering Sea. Part I: Classification*

S. N. RODIONOV

Joint Institute for the Study of the Atmosphere and Oceans, University of Washington, Seattle, Washington

J. E. OVERLAND

NOAA/Pacific Marine Environmental Laboratory, Seattle, Washington

N. A. BOND

Joint Institute for the Study of the Atmosphere and Oceans, University of Washington, Seattle, Washington

ABSTRACT

The Aleutian low is examined as a primary determinant of surface air temperature (SAT) variability in the Bering Sea during the winter [December–January–February–March (DJFM)] months. The Classification and Regression Tree (CART) method is used to classify five types of atmospheric circulation for anomalously warm months (W1–W5) and cold months (C1–C5). For the Bering Sea, changes in the position of the Aleutian low are shown to be more important than changes in its central pressure. The first two types, W1 and C1, account for 51% of the "warm" and 37% of the "cold" months. The W1-type pattern is characterized by the anomalously deep Aleutian low shifted west and north of its mean position. In this situation, an increased cyclonic activity occurs in the western Bering Sea. The C1-type pattern represents a split Aleutian low with one center in the northwestern Pacific and the other in the Gulf of Alaska. The relative frequency of the W1 to C1 types of atmospheric circulation varies on decadal time scales, which helps to explain the predominance of fluctuations on these time scales in the weather of the Bering Sea. Previous work has noted the prominence of multidecadal variability in the North Pacific. The present study finds multidecadal variations in frequencies of the W3 and C3 patterns, both of which are characterized by increased cyclonic activity south of 51°N. In general, the CART method is found to be a suitable means for characterizing the wintertime atmospheric circulation of the North Pacific in terms of its impact on the Bering Sea. The results show that similar pressure anomaly patterns for the North Pacific as a whole can actually result in different conditions for the Bering Sea, and that similar weather conditions in the Bering Sea can arise from decidedly different large-scale pressure patterns.

1. Introduction

The Aleutian low is the dominant feature of the atmospheric pressure system in the northern North Pacific during winter. Variability in strength and the position of the low is important to the Bering Sea through its impact on circulation, surface heat fluxes, mixed layer depths, and the extent of ice cover, all of which influence the rich biological resources of the sea (Wooster and Hollowed 1995; Wyllie-Echeverria and Wooster 1998; Hollowed et al. 2001; Benson and Trites 2002). Because the oceanic circulation over the shelf region of the eastern Bering Sea is so sluggish, the winter atmospheric circulation is considered to be the primary driving force behind the interannual variability of the oceanic environment of the region (Niebauer et al. 1999; Stabeno et al. 2001).

Previous work has found that warmer-than-normal winters in the Bering Sea tend to be associated with an anomalously strong Aleutian low (Niebauer 1983; Niebauer et al. 1999). Stabeno et al. (2001) explain this relationship through a tendency of individual storm systems that preferentially pump warm air poleward. This effect can be modulated by the mean meridional wind anomalies that can also accompany changes in the po-

Corresponding author address: S. N. Rodionov, Joint Institute for the Study of the Atmosphere and Oceans, Box 354235, University of Washington, Seattle, WA 98195-4235.
E-mail: sergei.rodionov@noaa.gov

sition and strength of the Aleutian low. Luchin et al. (2002) note that during warm winters the Aleutian low is not only about 3–6-hPa deeper than normal, but its center is shifted 3°–6° north and 10°–20° west of its long-term mean position.

The mechanism responsible for colder-than-normal winters in the Bering Sea is less well understood than that for the warmer-than-normal winters. Niebauer (1988, 1998) relates the anomalously cold winters to a weakening and retreat of the Aleutian low toward the west-northwest, allowing high pressure from the Asian high to dominate, which results in the cooling of the Bering Sea. This relationship is in apparent contradiction with the results of Rogers (1981) and Luchin et al. (2002). Rogers (1981) notes that Bering Sea ice extends farther south when St. Paul (Pribilof Islands, Alaska) is colder and the Aleutian low is farther east and deeper than normal. According to Luchin et al. (2002), anomalously cold winters occur when the Aleutian low is displaced east of its normal position, irrespective of its strength. Niebauer (1998) also notes that if the Aleutian low shifts well to the east (as during some strong El Niño events, especially after the regime shift of 1977), low-level winds over the Bering Sea blow from the east and north off of Alaska, resulting in above-normal ice conditions.

As indicated above, the relationship between the Aleutian low and Bering Sea winter climate conditions is far from being simple and straightforward. Different storm tracks and atmospheric pressure patterns in the North Pacific are often associated with the same sign of surface air temperature (SAT) anomalies in the Bering Sea. An example is provided by the cyclone density classification of Anderson and Gyakum (1989). Their 1+ type regime shows a well-defined zonal track maximum across the central North Pacific, as exemplified by the period of 15 January–13 February 1977. The 500-hPa means for this period represent a pattern with a deeper-than-normal low in the eastern and central North Pacific, accompanied by a strong west coast ridge. The opposite regime, the 1− type (as exemplified by the period of 8 February–10 March 1982), shows a split-track pattern with well-defined cyclone tracks in the eastern and western parts of the North Pacific; but, very few storms traverse the central part of the region, which is occupied by a strong 500-hPa ridge. Both of these periods, however, are characterized by positive SAT anomalies at St. Paul.

Mock et al. (1998) identify 13 major atmospheric circulation patterns that occur over Beringia. Their Siberia positive and Siberia negative types, for example, are opposite synoptic patterns, but the temperature and precipitation responses are not perfectly opposite between these two patterns, with both having negative SAT anomalies in the Bering Sea. From a different perspective, subtle shifts of circulation patterns can dramatically alter the spatial variations of surface climatic responses. Thus, both the north-central Pacific negative

and northeast Pacific negative types, classified by Mock et al. (1998), feature a strengthened Aleutian low positioned just a few degrees apart. Nevertheless, while the former is associated with generally warmer-than-normal temperatures throughout most of Beringia, the latter has positive SAT anomalies only over Alaska and negative anomalies over Siberia and the Bering Sea.

There are a number of indices that can be used to measure the state of the Aleutian low. Some of these indices are designed to be direct measures of Aleutian low variability, while others characterize a general character of atmospheric circulations over the North Pacific. Also, there are some indirect measures that are closely associated with the Aleutian low either through teleconnections or ocean–atmosphere interaction. A list of such indices, along with their brief definitions, is given below.

- *The North Pacific (NP) index.* This index is the area-weighted sea level pressure (SLP) over the region of 30°–65°N, 160°E–140°W (Trenberth and Hurrell 1994).
- *The Aleutian Low Pressure (ALP) index.* This is calculated as the mean area (km^2) with sea level pressure lower than or equal to 1005 hPa and is expressed as an anomaly from the 1950–97 mean (Beamish et al. 1997).
- *The Pacific Circulation (PC) index.* This index is a cumulative sum of negative northwesterly atmospheric circulation frequency anomalies: Z (westerly), M1, (northwesterly), and M2 (southwesterly) for December–March (King et al. 1998).
- *The Pacific decadal oscillation (PDO) index.* This is derived as the leading principal component of monthly sea surface temperature (SST) anomalies in the North Pacific, poleward of 20°N. The warm (cold) phase of the PDO is associated with a deepened (weakened) Aleutian low (Mantua et al. 1997).
- *The Atmospheric Forcing (AF) index.* This utilizes standardized scores of the first component from a principal components analysis on the ALP and PDO indices and the northwesterly atmospheric circulation anomalies for the North Pacific (December–March). Positive values represent the intense Aleutian lows, above-average frequency of westerly and southwesterly winds, cooling of sea surface temperatures in the central North Pacific, and warming within North American coastal waters (McFarlane et al. 2000).
- *The Pacific–North American (PNA) index.* A positive (negative) PNA index indicates an intensified (suppressed) Aleutian low. Overland et al. (1999) found that the correlation coefficient between the January–February Aleutian low central pressure and PNA index was $r = -0.77$ for the period of 1959–96.
- *The Southern Oscillation (SO) index.* The relationship between El Niño–Southern Oscillation (ENSO) events and the Aleutian low has been known since the mid-1960s (Bjerknes 1966). During El Niño win-

ters, the Aleutian low tends to be located southeast-ward of its usual position and averages about 2 hPa lower in central pressure. During La Niña winters, the Aleutian low is typically displaced westward of its usual position and is about 3 hPa higher in central pressure (Niebauer et al. 1999).

Simple correlation of these indices with Bering Sea ice cover and mean winter (DJFM) SAT anomalies at St. Paul (Table 1) suggests a lack of any strong linear relationships. The highest correlation coefficient of 0.37 was between the PDO index and SAT anomalies. This index, however, has a significant autocorrelation and, given the effective degrees of freedom, the value of the correlation coefficient does not exceed the 95% significance level. As we will show below, the reason for the lack of correlation is that the indices reflect the intensity of the Aleutian low rather than its geographical position, and the Bering Sea climate is much more responsive to the latter than to the former.

The Classification and Regression Tree (CART) method is employed here to diagnose the relationships between the large-scale atmospheric structure over the North Pacific, as encapsulated by the characteristics of the Aleutian low and winter conditions in the eastern Bering Sea. The CART method accounts for both the strength and position of the Aleutian low, and those circumstances for which it is split into two centers. It can also account for how a similar characteristic of the Aleutian low, in this case a location south of its long-term average position, can have different impacts in different periods. By better characterizing the true nature of the variability of the Aleutian low, the results from CART are less subject to the ambiguities associated with the simple indices itemized above. The paper is organized as follows: CART is briefly described in section 2, along with the data used. Section 3 discusses the tree-structured relationship between the characteristics of the Aleutian low and SAT anomalies in the Bering Sea, based on the data for the period of 1950–2002. Then, in section 4 this relationship is verified on the independent dataset for the period of 1916–49. Section 5 examines the composite maps of SLP, 500-hPa height, and SAT anomalies for each type of atmo-

spheric circulation; and section 6 analyses temporal variations in the frequency of these types. The results presented here demonstrate the multiplicity of circulation patterns that lead to anomalously warm and cold conditions in the Bering Sea.

2. Data and method

We used two sources of SLP data to measure the characteristics of the Aleutian low. The first source is the National Centers for Environmental Prediction (NCEP)–National Center for Atmospheric Research (NCAR) reanalysis dataset that has a 2.5° latitude × 2.5° longitude grid and begins in January 1948 (Kalnay et al. 1996). The second data source is the Northern Hemisphere Sea Level Pressure (NHSLP) dataset on a 5° × 5° grid from NCAR (Trenberth and Paolino 1981). The central pressure and geographical position of the Aleutian low were taken from the contour maps drawn on these data with a 1-hPa interval for the winter months from December through March. In those cases when the Aleutian low was split, the measurements were taken for both centers. The reanalysis data for the period from December 1949 to March 2002 were used for model development, while the NHSLP data for the period from January 1916 to March 1949 were used for model validation.

The long-term mean geographic position of the Aleutian low depends on the way it is calculated. On the mean winter SLP map (Fig. 1) the minimum pressure is found at approximately 52°N, 175°E. If, however, we first measure the position of the low for each winter month and then calculate averages for the entire period of observations, the result will be different. Considering all of the months with the Aleutian low having just one center, its average position is at 52°N, 176°W, which is marked by a diamond in Fig. 1. In those cases when the Aleutian low is split, one center is usually located near

TABLE 1. Correlation coefficients between the Aleutian low–related indices and Bering Sea ice cover and SAT anomalies.

Index	Ice cover*	SAT**
NP	0.03	−0.16
ALP	0.01	0.17
PC	0.12	0.02
PDO	−0.29	0.37
AF	−0.09	0.27
PNA	0.01	0.13
SO	0.05	−0.18

 * Annual maximum ice cover anomalies from 1972 to 2002.
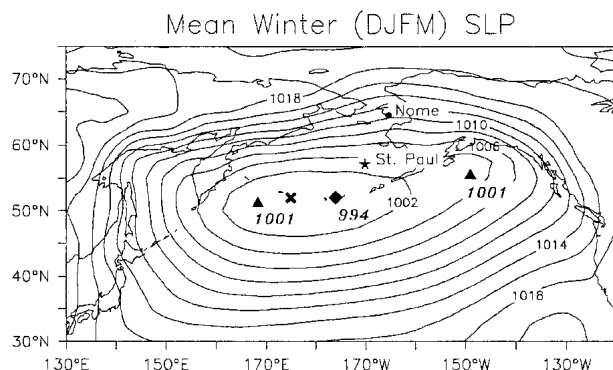** Mean winter (DJFM) anomalies from 1950 to 2002.

FIG. 1. Mean winter (DJFM) SLP in hectopascals averaged for the period of 1950–2002. The minimum SLP is marked by a cross. The mean position of the Aleutian low for nonsplit cases is marked by a diamond. The mean positions of the low pressure centers for split cases of the Aleutian low are marked by triangles. The position of St. Paul is indicated by a star.

51°N, 168°W, while the other in the Gulf of Alaska at 55°N, 149°W (triangles in Fig. 1). During the period of 1950–2002, the Aleutian low was split in 40% of all winter months with SLP being, on average, about the same in those two centers (1001 hPa). Overall, these two centers tend to strengthen and weaken simultaneously; the correlation coefficient between their central pressure values is $r = 0.45$ (significant at the 99% level).

Figure 1 suggests that the degree of seasonal averaging may affect the position of the Aleutian low and, thereby, the strength of its correlation with the central pressure. For example, if all of the months of a given winter feature a well-defined Aleutian low with one center, then on the mean winter map this center will likely be near its most frequent longitudinal position between the date line and 170°W. On the other hand, if some winter months have a split Aleutian low, while others do not, there is a good chance that those months being combined will produce a mean winter map with a relatively weak and westward-shifted Aleutian low. This creates an impression of a westward (eastward) movement of the Aleutian low as it gets weaker (stronger). In fact, Overland et al. (1999) found that the unsmoothed January–February mean values of longitude and central pressure of the Aleutian low were correlated at $r = -0.52$, with lower central pressures associated with locations farther east. If we consider only the months with a nonsplit Aleutian low, the strength of the correlation markedly weakens ($r = -0.27$), although it still remains significant at the 95% level.

To characterize winter temperature conditions in the eastern Bering Sea we used monthly SAT anomalies at St. Paul. There were two sources of the SAT data. One dataset (SAT_{PMEL}) was comprised from raw daily observations (taken from the airport) available from the National Oceanic and Atmospheric Administration (NOAA)/Pacific Marine Environmental Laboratory (PMEL) for the period of 1950–2002 (courtesy of D. Kachel). Another dataset (SAT_{GISS}) represents mean monthly values for the period of 1916–2002 obtained from the National Aeronautics and Space Administration (NASA) Goddard Institute for Space Studies (GISS). The two datasets are highly correlated ($r > 0.99$ for the overlapping period), but the SAT_{PMEL} values tend to be 0.3°C–0.4°C higher than the corresponding SAT_{GISS} values. The difference between the two datasets in some month may range from $-0.89°$ (with SAT_{PMEL} indicating colder conditions than SAT_{GISS}) to 1.10°C. The SAT_{PMEL} dataset was used for model development (1950–2002) and the SAT_{GISS} dataset for model verification (1916–49).

Figure 2 shows that SAT_{PMEL} in St. Paul is a good indicator of temperature conditions in the entire eastern Bering Sea, with the correlation coefficients exceeding 0.7 over most of the area. The SAT_{PMEL} time series is presented in Fig. 3. The monthly variations of normalized SAT anomalies are only weakly correlated, with the maximum correlation coefficient of 0.31 be-
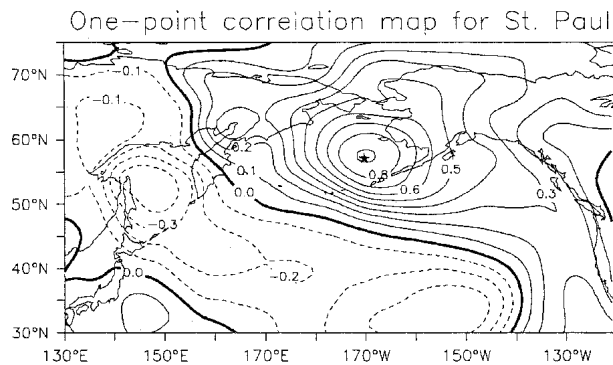

FIG. 2. One-point correlation map between mean winter (DJFM) SAT_{PMEL} anomalies in St. Paul and gridded SATs from the NCEP–NCAR reanalysis for the data period of 1950–2002.

tween February and March anomalies. December was the month most different from other winter months. For example, the cold period of the early 1970s, observed in all other months, was not that evident in December. The past decade saw extreme variability in December temperatures when the record cold month of December 1999 (negative SAT anomaly exceeded 3 std dev) was followed by the record warm month of December 2000. This variability occurs on a background of an overall cooling trend since the mid-1980s. The increasing frequency of negative temperature anomalies is also characteristic of January. In contrast, SAT anomalies in February and March have remained mostly positive since the North Pacific climate shift of 1977. Figure 3 also shows mean winter (DJFM) SAT anomalies, which are highly correlated with ice cover ($r = 0.87$). As for the correlation of mean winter SAT anomalies with individual months, the highest correlation coefficient is for January ($r = 0.72$), and the lowest is for December ($r = 0.16$).

For the purpose of our analysis we separated all of the monthly normalized SAT_{PMEL} anomalies into three categories—"cold" (≤ -0.32 standard deviation), "normal" ($-0.32 \ldots 0.43$ standard deviation), and "warm" (>0.43 standard deviation)—with approximately equal number of cases in each category. There were total of 72 cold, 73 warm, and 66 normal months. Then, we employed the CART method to classify atmospheric circulation patterns (based on the Aleutian low parameters) that are characteristic of the two extreme categories. The core of this method is a binary tree-growing algorithm developed by Breiman et al. (1984). Burrows and Assel (1992) were probably the first who used this technique in the field of hydrometeorology. They developed a tree-based statistical model for predicting daily ice cover on Lakes Superior and Erie. Describing the advantages of the method, they note that the resultant classification rules nearly always make clear physical sense. Hughes et al. (1993), Zorita et al. (1995), and Zorita and von Storch (1999) used the CART analysis to seek optimal statistical "downscaling" relationships between the large-scale
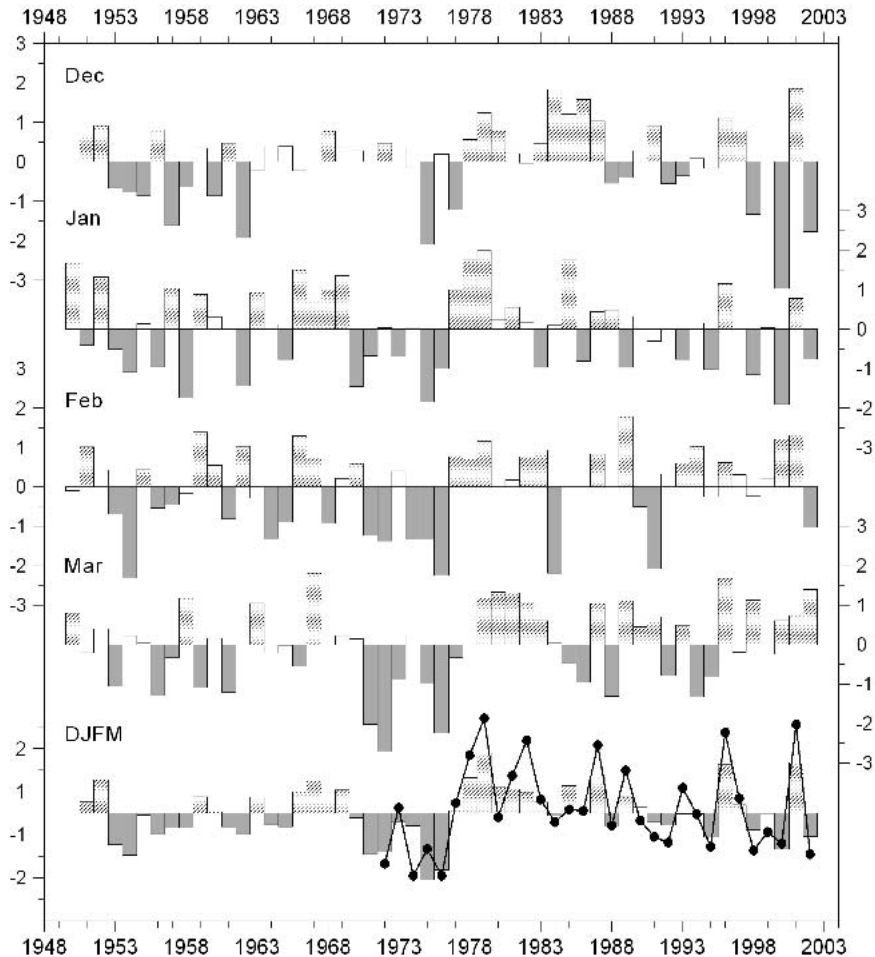
FIG. 3. Normalized (by standard deviation) mean monthly and mean winter (DJFM) anomalies of SAT in St. Paul (bar charts) for 1950–2002, and maximum ice cover extent along 169°W in the Bering Sea for 1972–2002. SAT anomalies for Dec are shifted 1 yr forward to facilitate their comparison with other winter months (e.g., Dec 2001 is plotted against the year 2002).

circulation and local daily precipitation. In this application the CART analysis searches recursively for a binary decision tree with the decision nodes that are based on the values of the large-scale atmospheric variables at some key locations or the values of key large-scale atmospheric indices. Each terminal node of the tree represents a weather state. To reduce the dimensionality of the problem, the input variables for the CART analysis can be the leading EOFs of the SLP field. New daily SLP anomaly fields, observed in another period or simulated by a CGM, can be classified into one of these states and the local rainfall that is attached to this circulation can be chosen at random from all of the days belonging to that particular weather state.

Rodionov and Assel (2000) applied CART to a classification problem (categorical target variable) on a longer interannual time scale. They developed a simple characterization of warm, normal, and cold winters in the Great Lakes in terms of teleconnection indices and their combinations. They found this method to be par-

ticularly useful when a relationship between the target variable and predictors are not necessarily symmetric with respect to the sign of anomaly. Specifically, warm winters in the Great Lakes basin are strongly associated with El Niño events, while the association between cold winters and La Niña events is much weaker.

In the present work we take advantage of CART's ability to process different kinds of information (both quantitative and qualitative), such as whether the Aleutian low has one or two centers. The input variables for the CART analysis were central pressure and geographic coordinates of the Aleutian low, and the target variable was the categories of SAT anomalies at St. Paul. As in Rodionov and Assel (2000), the Gini index of impurity (Breiman et al. 1984) was used as a node-splitting criterion in the process of growing the classification tree. For an overview of the algorithm and discussion of CART advantages over other classification methods, see Rodionov and Assel (2000).

A major issue that arises when applying CART to

real data with noise concerns the decision of when to stop splitting. This problem of "overlearning" or "overfitting" is common to all other methods of statistical modeling. If not stopped, CART will continue splitting until all cases are perfectly classified, resulting in a tree structure that is as complex as the original data, with many nodes possibly containing just single observations. Such an unreasonably big tree would only make the interpretation of the results more difficult, and most likely it would not be very useful or accurate for classifying new observations. Therefore, there is always a trade-off between the size of a tree and impurity of its nodes.

Typically, the splitting of tree nodes will continue until one of the stopping rules is triggered, for example, when the depth of the tree reaches its prescribed maximum value or the decrease in impurity is less than a prescribed value. There are many situations, however, when these stopping rules do not work well. Depending on the threshold, the splitting may either stop too soon at some terminal node or may continue too far in other parts of the tree. Breiman et al. (1984) recommends continuing the splitting until sample sizes in the nodes become very small, and then selectively pruning the tree back.

Another strategy, adopted here, is to grow the tree to just the right size, where the right size is determined by the user, based on the knowledge from previous re-search, diagnostic information from previous analyses, or even intuition. This approach involves a number of experiments, which results in a set of trees. These experiments make sense because CART is only one-step optimal and not overall optimal. The final tree chosen from this set should have a low misclassification error and be as small as possible. It should be physically sound and lead to a better understanding of the phenomena it describes. Admittedly, this method is quite subjective. Therefore, when the amount of data allows, it is useful to further evaluate the quality of the tree via cross validation, that is, it is helpful to apply the tree computed from one set of observations (learning sample) to another completely independent set of observations (testing sample).

3. Classification tree

The first split of the classification tree was forced whether the Aleutian low represented one or two centers. This seems logical because these are two qualitatively different situations. It is worth noting that CART itself suggests that the root node be split on the longitude of the Aleutian low (single center) and that there should be a separation of 13 cold, 2 normal, and 1 warm month in one node (same as node C2 in Fig. 4). Further
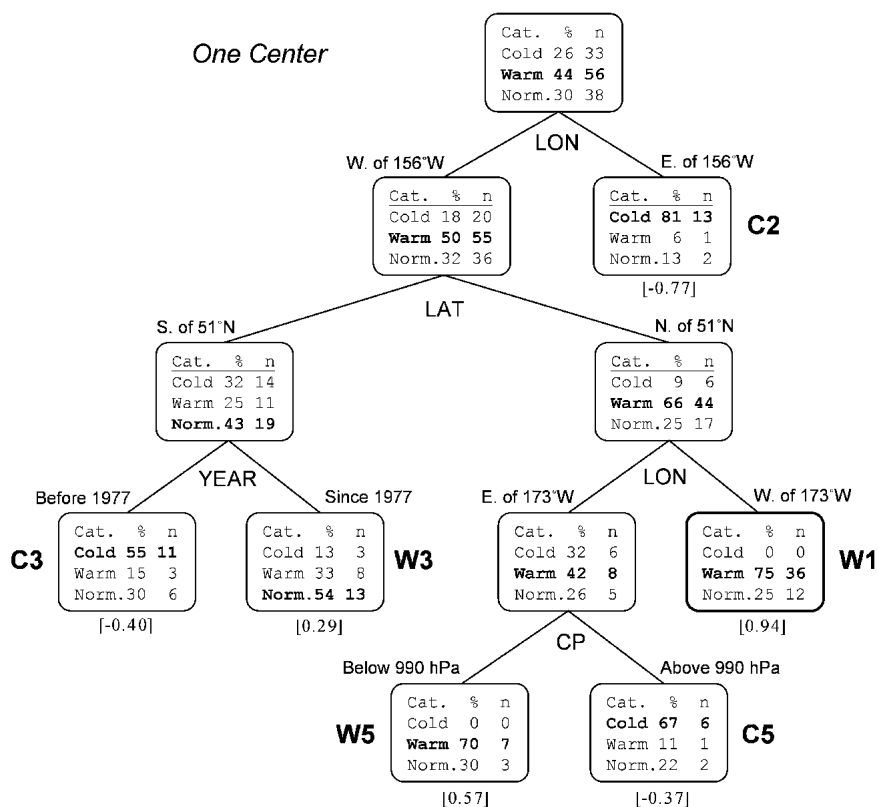

FIG. 4. A branch of the classification tree for the cases of a nonsplit Aleutian low, 1950–2002. Numbers in square brackets under each terminal node are mean monthly values of normalized (by the standard deviation) SAT anomalies in St. Paul averaged for the months in the nodes.

splits, however, lead to an oversized, poorly structured tree with a higher misclassification error than the one described below. Most importantly, this fully automatic procedure could not produce two major nodes, W1 and C1, containing large portions of warm and cold months, respectively, with a surprisingly high degree of purity of these nodes.

Two separate branches of our best tree, corresponding to the situations of one and two centers in the Aleutian low, are presented in Figs. 4 and 5 respectively. All of the other nodes of this tree were split as recommended by CART. Each terminal node of the tree represents a type of atmospheric circulation associated with either a warm or cold category of SAT anomalies, depending on which one dominates in the node. There was a total of five terminal nodes (types) for the warm (W1–W5) and five for the cold (C1–C5) categories. The numbers in brackets below the terminal nodes are mean SAT anomalies for all of the months in those nodes. Table 2 lists warm and cold months for two major types of atmospheric circulation (W1 and C1), and Tables 3 and 4 do so for the W2–W5 and C2–C5 circulation types, respectively. Misclassified months are given in italics.

a. One center

Figure 4 shows a branch of the tree when the Aleutian low represents a single, well-defined center. When this is the case, the odds of a warm versus a cold month in the Bering Sea increase from roughly equal to 1.7:1
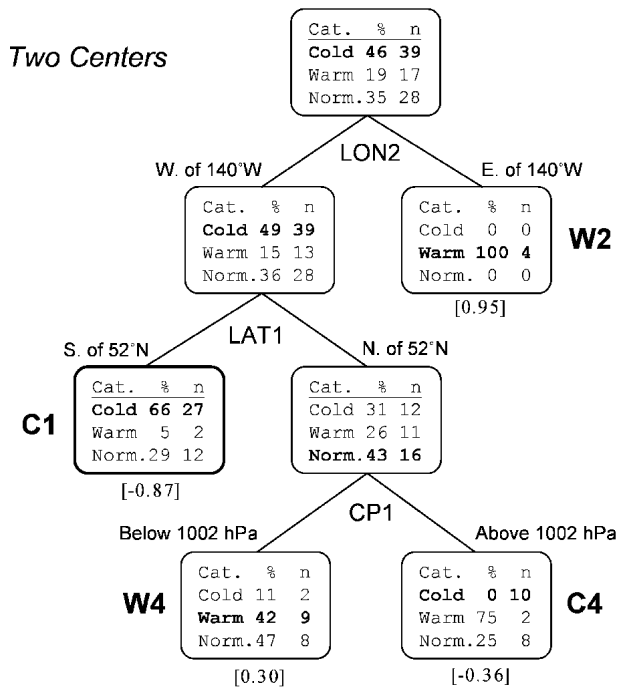
TABLE 2. A list of warm and cold months in the terminal nodes W1 and C1, respectively. Misclassified warm months in the C1 node are given in italic.

W1		C1	
Mar 1950	Jan 1979	Jan 1951	Jan 1973
Feb 1951	Mar 1980	Jan 1954	Feb 1974
Dec 1951	Dec 1983	Feb 1956	Dec 1974
Feb 1955	Dec 1984	Dec 1956	Jan 1975
Jan 1957	Jan 1985	Feb 1957	Feb 1976
Mar 1958	Dec 1985	Mar 1959	Mar 1976
Feb 1959	Dec 1986	Feb 1961	Feb 1984
Feb 1960	Mar 1987	Dec 1961	Jan 1986
Dec 1960	Jan 1988	Jan 1962	Feb 1991
Feb 1962	Feb 1989	Feb 1965	Jan 1993
Jan 1966	Dec 1990	Jan 1971	Mar 1995
Feb 1966	Mar 1991	Mar 1971	Jan 1998
Mar 1967	Mar 1993	Feb 1972	Dec 1999
Jan 1968	Mar 1996	Mar 1972	
Jan 1969	Feb 2000		
Feb 1970	Dec 2000		
Jan 1978	Feb 2001		
Dec 1978	Mar 2002	*Feb 1994*	*Mar 2001*

(56 warm versus 33 cold winters), or, in terms of probabilities, the probability of a warm month increases by 13% (from 50% to 63%), whereas the probability of a cold month decreases by 13%. Most of the warm months (56 out of total 73, or 77%) went through this branch. What becomes important next in a separation of warm and cold month is the longitudinal position of the Aleutian low. When the center of the low is east of 156°W, that is, basically, in the Gulf of Alaska, it is almost certainly cold in the eastern Bering Sea. There are 13 cold months and just 1 warm month in this terminal node that is marked as C2. During this misclassified warm month (March 1989) the Aleutian low was weaker (1005 hPa in its center) and located farther south (50°N) and east (140°W) than during the rest of the months in this group.

When the Aleutian low is not in the Gulf of Alaska, its most important characteristic for discriminating warm and cold months is its latitudinal position. When the Aleutian low is north of 51°N (i.e., near or to the

FIG. 5. Same as Fig. 4, but for the cases of a split Aleutian low.

TABLE 3. A list of warm months in the terminal nodes W2 through W5. Misclassified cold months are given in italic.

W2	W3	W4	W5
Jan 1952	Jan 1977	Dec 1950	Feb 1977
Dec 1977	Feb 1978	Dec 1955	Jan 1981
Feb 1979	Mar 1979	Jan 1959	Mar 1981
Feb 1982	Mar 1983	Jan 1967	Dec 1982
	Feb 1987	Feb 1967	Feb 1983
	Feb 1993	Dec 1967	Mar 2000
	Dec 1995	Dec 1971	Jan 2001
	Jan 1996	Mar 1982	
		Feb 1996	
	Jan 1991	*Dec 1959*	
	Mar 1992	*Dec 1987*	
	Jan 1995		

TABLE 4. A list of cold months in the terminal nodes C2 through C5. Misclassified warm months are given in italic.

C2	C3	C4	C5
Dec 1952	Jan 1953	Mar 1953	Feb 1953
Jan 1958	Feb 1954	Dec 1954	Dec 1953
Mar 1961	Mar 1957	Jan 1956	Feb 1964
Mar 1966	Jan 1965	Mar 1956	Dec 1988
Jan 1983	Feb 1968	Dec 1957	Jan 1902
Mar 1985	Jan 1970	Mar 1975	Feb 1902
Mar 1986	Feb 1971	Mar 1977	
Mar 1988	Mar 1973	Jan 1989	
Feb 1990	Feb 1975	Dec 1992	
Dec 1991	Jan 1976	Jan 2000	
Mar 1994	Dec 1976		
Dec 1997			
Dec 2001			
Mar 1989	*Jan 1950*	*Dec 1979*	*Mar 1998*
	Jan 1963	*Dec 1996*	
	Mar 1963		

north of its long-term position) the chances for the eastern Bering Sea to be warmer than normal increases substantially. If, in addition to that, the Aleutian low is positioned west of 173°W (i.e., near or west of its long-term mean position for one center), the result is the most common type of atmospheric circulation (named here as W1) associated with warm winter months in the Bering Sea. The purity of this node is very impressive—it contains 36 (or, practically, 50% of the total 73) warm months and 0 cold months.

Two types of atmospheric circulation (W5 and C5) have much in common in terms of the geographical position of the Aleutian low. In both cases it is located north of 51°N and east of 173°W (but not in the Gulf of Alaska). The difference between the two types is in the central pressure. If the Aleutian low is deep (below 990 hPa), the advection along its eastern periphery is strong enough to bring warm Pacific air to the eastern Bering Sea. Otherwise, SAT anomalies there tend to be on the cold side.

There is one case when the split of the node is made not on the parameters of the Aleutian low, but on the variable "time" (years). When the Aleutian low is located south of 51°N, there are no simple characteristics that could provide a satisfactory separation of warm or cold months in the Bering Sea. It is clear, however, that before 1977, this position of the Aleutian low was more often associated with colder-than-normal conditions in the Bering Sea (type C3). Since 1977, the sea tends to be warmer than normal under these circumstances (type W3). The transition year coincides with the major shift in the Pacific climate (e.g., see Miller et al. 1994). It must be admitted that splitting the node based on years makes it difficult to validate the model on an independent dataset for a different period, or to use it for forecasting (classification of new observations). This tree, however, is considered as being a diagnostic, rather than a forecasting, model. Analyzing the difference between various aspects of W3 and C3 circulation

types may help to better understand the climate shift of 1977. The decision to split this node on years was reinforced when during the validation procedure on the independent dataset for 1916–49 (see below), the best variable for this purpose again was time.

b. Two centers

The branch of the classification tree for two centers of the Aleutian low (Fig. 5) is even shorter than for one center. As the root node for this branch demonstrates, the Bering Sea tends to be anomalously cold when the Aleutian low is split. There are 39 cold and 17 warm months in this node, that is, the odds are more than 2 to 1 in favor of there being colder-than-normal conditions in the Bering Sea.

The next step separates four warm months, the common feature of which is that the eastern center is too far east (east of 140°W) to affect the Bering Sea. This relatively rare type of circulation was termed W2.

The principal type of atmospheric circulation that is characteristic of anomalously cold months in the Bering Sea, C1, is associated with a southward excursion of the western center of the Aleutian low. If this center is located south of 52°N, that is, near to or south of its normal position, the probability of colder-than-normal conditions in the Bering Sea becomes very high, because the overwhelming majority of months in the C1 node belong to the cold category (27 versus only 2 warm months).

When the western center of the Aleutian low is located north of 52°N, that is, far north of its long-term position, its effect on temperature in the Bering Sea depends on the strength of this center. If its central pressure is below 1002 hPa, then the temperature tends to be above normal. If the pressure is above 1002 hPa, below-normal temperatures are favored.

4. Verification

Despite its simplicity, the classification tree discussed above correctly classifies 89% of all warm and 93% of all cold months in the Bering Sea. The question is, however, whether or not this tree is stable over time. In order to answer this question, we tested this tree on the independent data for the period of 1916–49. Here, we used the NHSLP dataset, which is on a larger grid (5° × 5°) than that of the NCEP–NCAR reanalysis (2.5° × 2.5°). This fact alone increases the possibility of errors because the standard deviation of the latitudinal position of the Aleutian low (nonsplit cases only) is just 2.8°, and even seemingly minor changes in its position may be important. Besides, the overall quality of data usually decreases further back in time. Nevertheless, even in these circumstances the classification tree turned out to be surprisingly stable and performed well on the independent data. In correctly classified 38 of the total 44 (86%) warm months, and 38 of the total 43 (88%) cold months for the 1916–49 period.

It is important to note that the split between W3 and C3 is based on years (Fig. 4), and that this split must be reevaluated in the testing sample. It turned out that the best split for this node, using the earlier, independent data, was also based on years. The periods of 1916–21 and 1938–49 were classified as C3, because the ratios of cold to warm months for these periods were 5–0 and 8–0, respectively. The period of 1922 through 1937 was classified as W3, because the ratio of warm to cold months for this period was 12–2. Hence, the split rule for this node for the entire period of 1916–2002 can be written as

$$\text{IF YEAR} < 1922 \text{ OR } 1937 < \text{YEAR}$$

$$< 1977 \text{ THEN C3, ELSE W3.}$$

In other words, when the Aleutian low was centered south of 51°N and west of 156°W, the response of the Bering Sea was different in different periods. Prior to 1922 and from 1938 through 1976, this situation was most often associated with below-normal temperatures in the Bering Sea (type C3). From 1922 through 1937, and since 1977 through at least 2002, the same situation was associated with above-normal temperatures in the sea (type W3).

In order to evaluate the ability of the tree to model temporal variability of SAT at St. Paul, each terminal node in Figs. 4 and 5 was assigned an average normalized SAT anomaly for all of the months in the node. To characterize SAT variability within the nodes, the upper and lower quartiles of SAT distributions for each node were also calculated. The modeled time series was then compared with the observed temperature anomalies for both the model-development and independent datasets. Table 5 shows the correlation coefficients between the two time series that were calculated for monthly and seasonal values. Although the correlation coefficients are somewhat lower for the independent data (particularly for monthly means), they still remain significant at the 99% level.

The modeled and observed mean winter (DJFM) SAT anomalies at St. Paul are presented in Fig. 6. Both time series demonstrate good agreement, both in the year-to-year variations and in terms of warming and cooling trends. Thus, for the independent data (1916–49), the model reproduced reasonably well a warming trend from the late 1910s through the 1930s, and a cooling trend in the 1940s. The largest error was in 1937— the warmest year on record. This error occurred due to

TABLE 5. Correlation coefficients between modeled and observed SAT anomalies at St. Paul. Number of observations is given in parentheses.

Period	Monthly means	Winter means
1916–49	0.58 (129)	0.64 (31)
1950–2002	0.69 (211)	0.67 (53)
1916–2002	0.65 (340)	0.66 (84)

a significant misclassification of 2 months of this year: February and March. During both of these months the Aleutian low was split into two weak centers, one in the Gulf of Alaska and the other at about 165°W. The latitudinal position of the western center was at 55°N in February and 51°N in March. As a result, the February pattern was classified as C4, with the average SAT anomaly of −0.36, and the March pattern was classified as C1, with the average SAT anomaly of −0.87. Meanwhile, observed SAT anomalies were +1.7 standard deviation in each of these months. It should be noted, however, that February and March of 1937 appear to be among those months that are characterized by strong spatial gradients and overall inhomogeneity of SAT anomalies in the Bering Sea. In fact, SAT anomalies in Nome Alaska, in the northeastern part of the sea (Fig. 1) were below average for the 1916–49 period (−0.5 standard deviation in February and −0.7 standard deviation in March 1937).

5. Composite maps

The composite maps of SLP, 700-hPa heights, and their anomalies, as well as the associated SAT anomalies, are shown here for all of the types of atmospheric circulation that were classified in section 3. We will start with the two basic types, W1 and C1, which are characteristic of the majority of warm and cold months in the eastern Bering Sea, respectively, and then discuss the rest of the types.

a. Basic types

The basic type of atmospheric circulation for anomalously warm winter months in the Bering Sea, W1, is characterized by a well-defined Aleutian low with the central pressure of 998 hPa (Fig. 7a). This is 3 hPa *below* the normal value of the mean winter central pressure in the Aleutian low, but is 4 hPa *above* the long-term central pressure if only nonsplit cases of the Aleutian low are taken into account (Fig. 1). Geographically, the Aleutian low in this pattern is shifted about 1° north and 12° west of this latter center (marked by a diamond in Fig. 1). The direction of the shift is consistent with the results of Luchin et al. (2002), but the values here are much smaller.

It is interesting to compare the SLP pattern of the W1 circulation type (Fig. 7a) with the Aleutian above (AA) mode of the North Pacific Oscillation (NPO) as described by Walker and Bliss (1932) and Rogers (1981). One can expect that the two patterns would have much in common because the definition of the AA mode includes well above normal temperatures at St. Paul. Although the W1 pattern indeed bears some resemblance to the AA mode (see Fig. 2 in Rogers 1981), the Aleutian low in W1 is much stronger. This is largely because the AA mode appears to be less homogeneous than W1 and includes other types of atmospheric circulation, such as W2 (e.g., January 1952) and

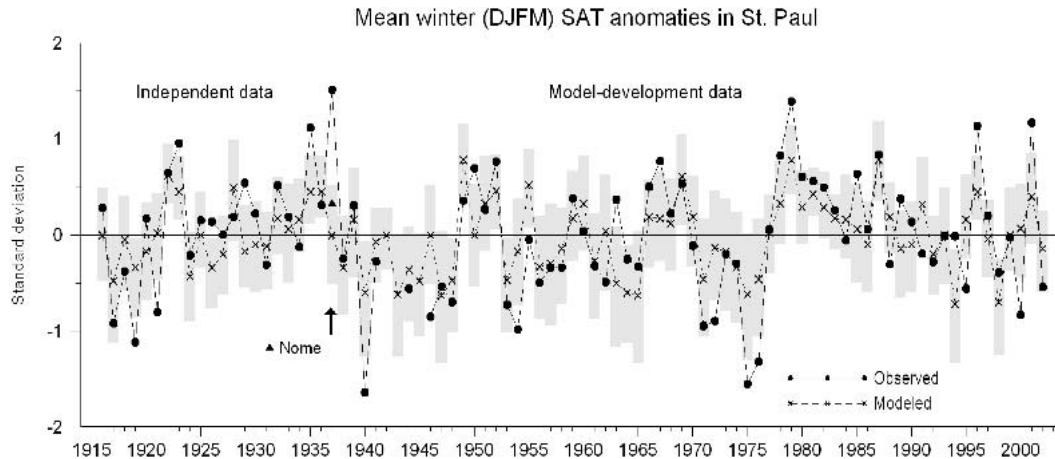Mean winter (DJFM) SAT anomalies in St. Paul

FIG. 6. Observed (solid line) and modeled (broken line) mean winter (DJFM) normalized SAT anomalies in St. Paul for the periods of independent (1916–49) and model-development (1950–2002) data. Gray bars indicate 50% quantiles of temperature distributions around the mean values.

W4 (e.g., January 1959), which are also associated with above-normal temperatures in St. Paul, but are characterized by a weaker-than-normal Aleutian low.

The northwestern shift of the Aleutian low under the W1 type of atmospheric circulation results in negative SLP anomalies centered over the western Bering Sea (Fig. 7b). This is indicative of more frequent storms entering the Bering Sea along the Siberian coast (Overland and Pease 1982). At the same time, cyclonic activity in the Gulf of Alaska is suppressed.

The 700-hPa field (Fig. 7c) features a deep cyclonic center over the Kamchatka Peninsula and a strong ridge over the American coast extending toward Alaska, which implies an amplification of the climatological trough/ridge system over the North Pacific. The ridge over Alaska suppresses storms in the Gulf of Alaska and tends to redirect them to the Bering Sea. Fang and Wallace (1994) have demonstrated that during blocking episodes over Alaska the ice edge tends to stagnate over in the Bering Sea, while it advances rapidly in the Sea of Okhotsk.

Although a strong ridge over the west coast of North America is one of the characteristic elements of the PNA pattern, the distribution of 700-hPa anomalies (Fig. 7d) does not resemble that pattern. Actually, it resembles neither any of the teleconnection patterns that are currently monitored by NOAA's Climate Prediction Center (CPC; information online at http://www.cpc.noaa.gov/data/teledoc/telecontents.html), nor the teleconnection patterns recognized by Wallace and Gutzler (1981). The dipole in Fig. 7d is somewhat similar to the leading mode obtained by Fang and Wallace (1994) from their singular value decomposition (SVD) analysis of the temporal covariance matrix between wintertime sea ice concentration over the Pacific sector and the hemispheric 500-hPa field (their Fig. 7b). Both circulation patterns feature strong southerly anomalous

winds over the Bering Sea and warmer-than-normal conditions with the maximum deviations in the eastern part of the sea (cf. Fig. 7e and their Fig. 7a). The difference between the patterns is that the eastern center of the dipole in Fig. 7d is about 10° south of its counterpart for the leading SVD mode. This is probably a result of the assumption of system linearity in the SVD analysis, when the positive and negative phases of the pattern are strictly symmetric. CART, on the other hand, is intrinsically nonlinear, and the opposite phases of the pattern are not necessarily the mirror images of each other. As shown below, the eastern center of the dipole for C1 is shifted farther north, compared to that for W1.

The SLP composite for the C1 type shows a split Aleutian low (Fig. 7f), the two centers of which are very weak. The central pressure in these centers exceeds not only the overall mean winter SLP in the center of the Aleutian low (Fig. 1), but the long-term mean values in the two centers if only split cases are taken into account. The pattern in Fig. 7f has little in common with the Aleutian below (AB) mode of the NPO (Rogers 1981). The latter represents an elongated center of less than 1000 hPa (i.e., deeper than that for the AA mode) centered at 50°N, 170°W. Again, the chief reason for the difference is a separation of C1 from other cold patterns, such as C2, C3, and C5, which are characterized by negative SLP anomalies over the eastern Aleutian Islands. A composite map that includes all cold months (not shown) is much closer to the AB mode.

The two centers in the SLP composite (Fig. 7f) are transformed into a field with one dominant center when the anomalies are calculated (Fig. 7g). In some sense, this is opposite to what we saw for the W1 type, when the Aleutian low representing one center (Fig. 7a) turned into a dipole on the SLP anomaly map (Fig. 7b). To estimate the degree of symmetry between the SLP
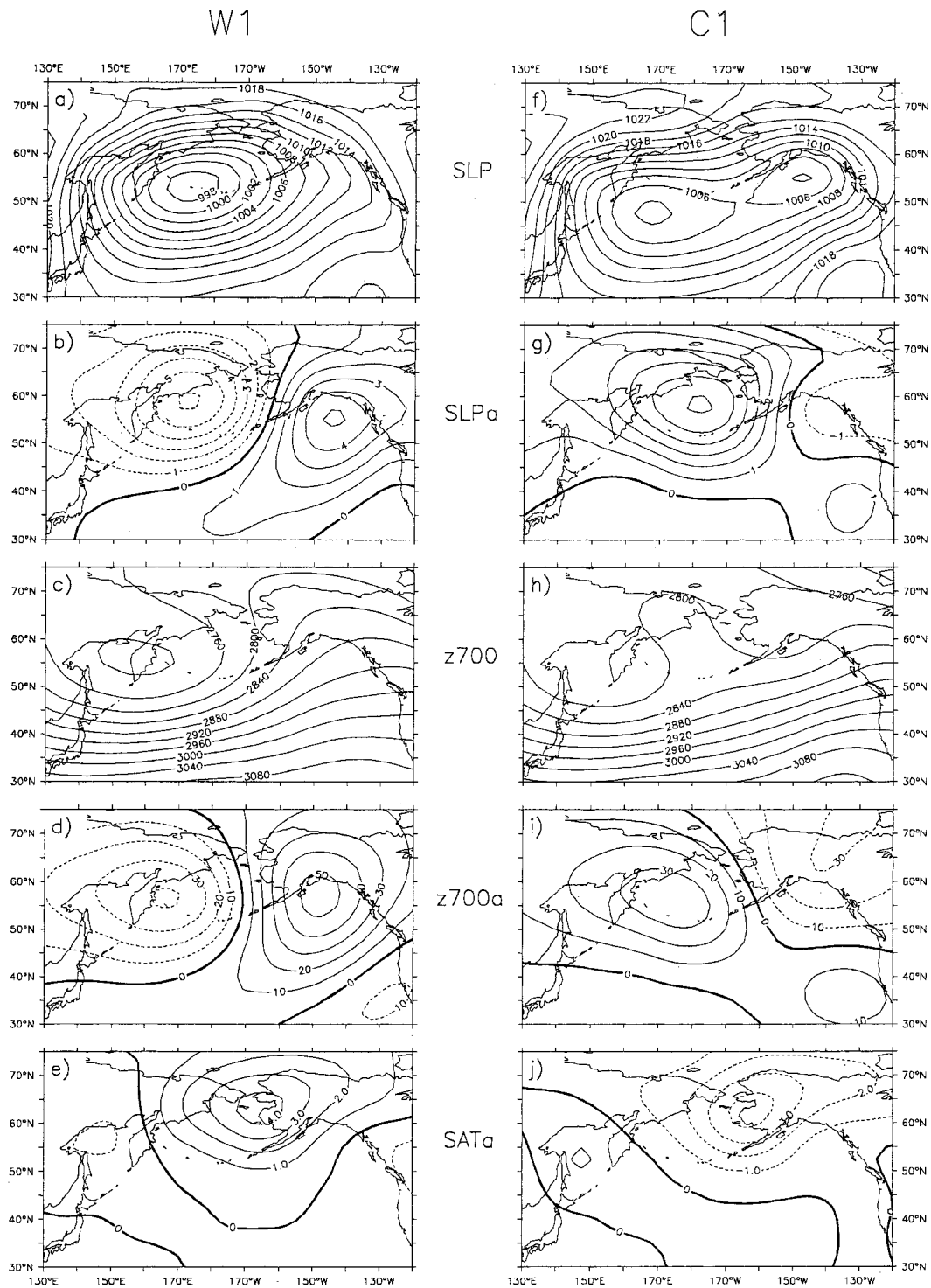
FIG. 7. Composite maps for the W1 and C1 types of atmospheric circulation. (a), (f) SLP and (b), (g) SLP anomalies are in hectopascals; (c), (h) 700-hPa geopotential height and (d), (f) height anomalies are in geopotential meters; and (e), (j) SAT anomalies are in degrees Celsius.

anomaly maps, we calculated the spatial correlation coefficient r_{sp} defined as

$$r_{sp} = \frac{\sum\limits_{i,j} w \cdot c}{\sqrt{\sum\limits_{i,j} w^2 \cdot c^2}},$$

where w and c are anomalies in grid points i, j for the warm and cold patterns, respectively. For the SLP anomaly fields (Figs. 7b and 7g), $r_{sp} = -0.76$, which means that, although there is a high degree of symmetry between these two fields, they are far from being the mirror images of each other. If we take the difference between the composite maps of SLP anomalies for the W1 and C1 types, the resultant pattern (not shown) will be much like the difference between the AA and AB modes of the NPO (Fig. 3 in Rogers 1981), except that the eastern center in the NPO dipole is stronger than the western one, while in our case it is the reverse.

The high pressure anomaly center in the Bering Sea (Fig. 7g) suggests an enhanced frequency of blocking activity in this region. At the 700-hPa level this is seen as an omega-type blocking (Fig. 7h). Renwick and Wallace (1996) found that the occurrence of blocking in the Bering Sea region was sensitive to the averaged polarity of the PNA pattern, but was even more sensitive to the phase of ENSO cycle. Sixty-nine percent more days of blocking were observed during winters occurring during the cool phase of ENSO, compared to those occurring during the warm phase. Niebauer (1983, 1988) also note that cool periods in the Bering Sea are associated with ridging in this area and advection of cold air along the eastern periphery of the ridge—a situation that is often coincident with cold ENSO events. It is important to underscore that the ridging involves only the high latitudes (north of 55°N), while the atmospheric circulation south of it (35°–55°N latitudinal band) remains zonal.

The corresponding 700-hPa anomaly field (Fig. 7i) resembles the Siberian pattern of Hsu and Wallace (1985). At the 1000-hPa level the Siberian pattern features a split Aleutian low as in our Fig. 7f. The spatial pattern of the difference between the 700-hPa anomaly composites for W1 and C1 (not shown) is similar to that for W1 itself (Fig. 7d), except that the eastern center of the dipole is shifted northward to Alaska, so that the pattern closely matches the leading SVD of Fang and Wallace (1994) for the North Pacific ice cover and hemispheric 500-hPa heights.

Interestingly, while many aspects of atmospheric circulation for the C1 type are simply opposite to those for the W1 type, there is still a significant degree of asymmetry between the corresponding SLP and 700-hPa height patterns, suggesting the overall nonlinearity in the system. Yet, the SAT composites in Figs. 7e and 7j are almost perfect mirror images of each other. The spatial correlation coefficient between these two composites is $r_{sp} = -0.93$.

b. Secondary types

Although the W1 and C1 types of atmospheric circulation are the most typical for the warm and cold winter months, respectively, they do not explain the whole variety of situations that may occur in the Bering Sea. Figure 8 shows four other warm patterns, W2–W5, and Fig. 9 shows four cold patterns, C2–C5. As one can notice, some of the warm patterns look much like C1, whereas some cold patterns resemble W1. Below we will briefly describe the characteristic features of those secondary patterns.

The W2 pattern (Figs. 8a–d) is a relatively infrequent type of atmospheric circulation. It occurred only four times during 1950–2002 and six times during 1916–49. It is very similar to the type "one minus" regime of Anderson and Gyakum (1989), and the Pacific pattern described by Hsu and Wallace (1985) and Renwick and Wallace (1996). As Hsu and Wallace (1985) note this pattern is also evident in the teleconnectivity map in Wallace and Gutzler (1981; Fig. 8) and has close resemblance to the NPO. Being similar to the C1 type, it features a split Aleutian low at sea level and a blocking ridge at the 700-hPa level. An important difference between the C1 and W2 patterns is that in the latter case the midtropospheric ridging embraces not only the high latitudes (north of 55°N), but also the central North Pacific. It means that the major Pacific storm track is effectively blocked and cyclones are deflected northward, along the Asian coast, as can be seen in Anderson and Gyakum (1989). The positive SAT anomaly (Fig. 8d) is centered over the eastern tip of Siberia, but includes most of the Bering Sea except the Bristol Bay.

The W3 pattern (Figs. 8e–h) is characteristic of warm ENSO events, when the Aleutian low strengthens and shifts south (or southeast) of its normal position (Bjerknes 1966, 1969; Niebauer 1998). The circulation associated with an intensified Aleutian low drives warm, moist air northward along the northeastern Pacific coast up over Alaska and the Bering Sea, as described in Niebauer (1988, 1998). The El Niño of 1976/77 is a good example of this type of circulation.

The SLP composite map for the W4 type (Fig. 8i) is largely the same as the composite map for La Niña events in Niebauer (1998) in terms of the strength and position of two low pressure centers. The 700-hPa anomaly map (Fig. 8k) features a strong high pressure cell in the central North Pacific, which is mostly a result of a general shift of the circulation zones to the north, rather than anomalous ridging, which is not that evident in Fig. 8j. It is interesting that, despite the overall opposition of the 700-hPa anomaly patterns for the W3 and W4 types ($r_{sp} = -0.71$), both are associated with positive SAT anomalies in the Bering Sea. The sources of warm air for these two types, however, are significantly different.

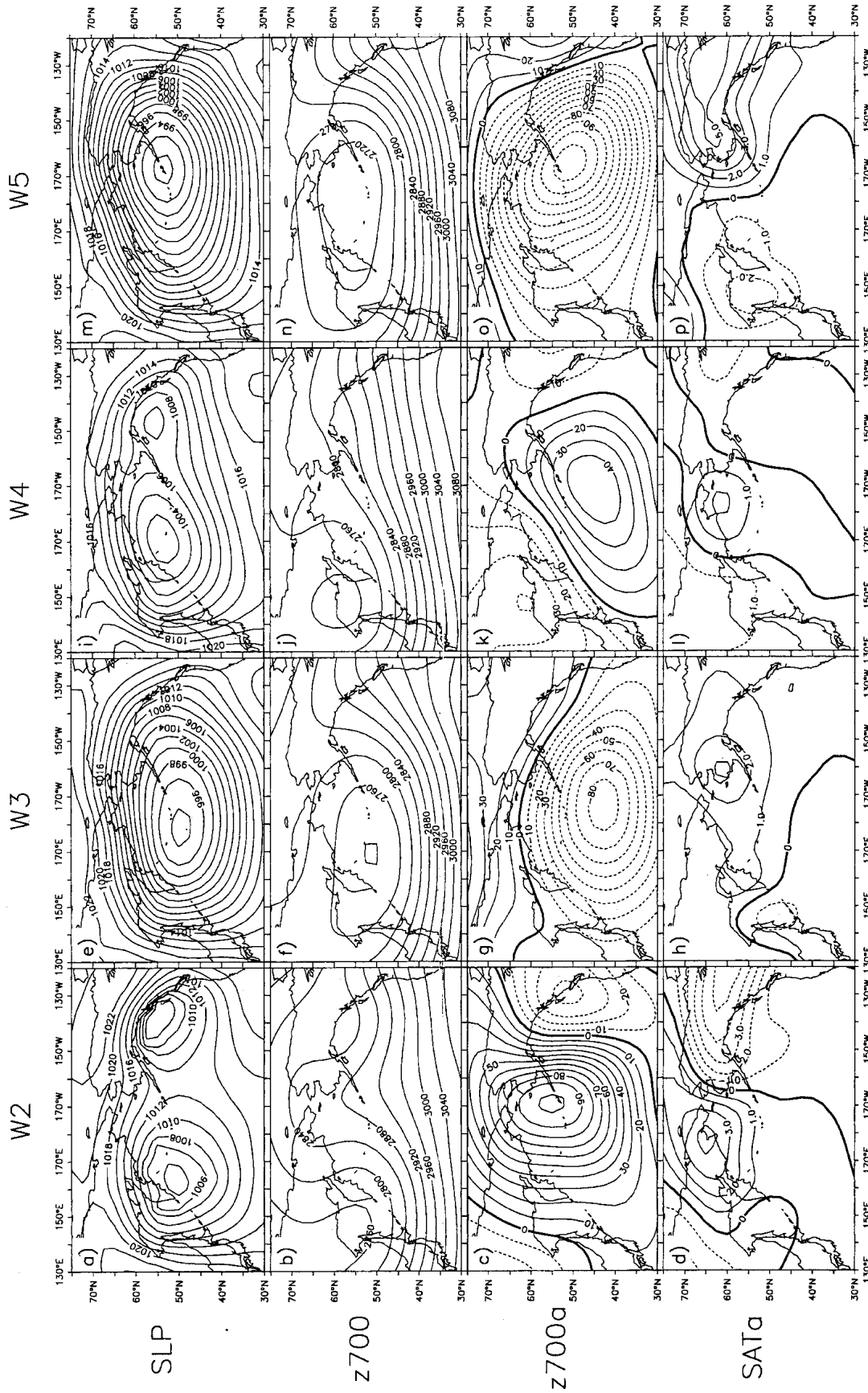During some strong El Niño events, such as the 1982/83 events, the Aleutian low strengthens and moves

FIG. 8. Composite maps for the W2–W5 types of atmospheric circulation. (a), (c), (i), (m) SLP is in hectopascals; (b), (f), (j), (n) 700-hPa geopotential height and (c), (g), (k), (o) height anomalies are in geopotential meters; and (d), (h), (l), (p) SAT anomalies are in degrees Celsius.
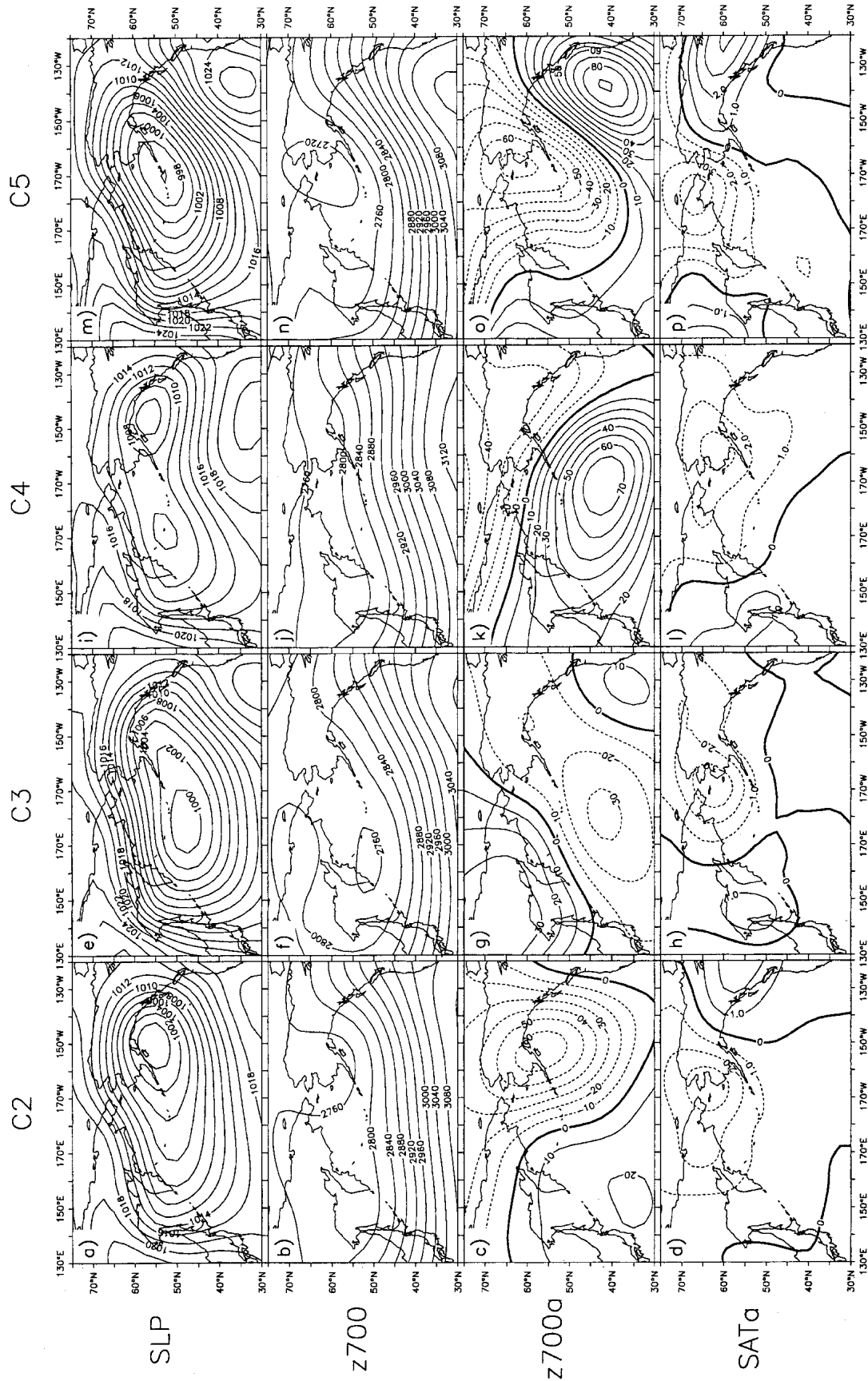
FIG. 9. Same as Fig. 8, but for the C2–C5 types of atmospheric circulation.

even farther eastward (east of 173°W) than during moderate El Niños, such as the 1976/77 event (e.g., Niebauer 1998). It cannot be, however, too far east (i.e., east of 156°W), because then the anomalous winds over the Bering Sea are northerly as in the C2 pattern discussed below. As the classification tree in Fig. 4 shows, when the Aleutian low is south of 51°N and between 156° and 173°W, the outcome for the SAT of the Bering Sea depends on the strength of the Aleutian low. The composites on Figs. 8m–p summarize the cases when the central pressure in the Aleutian low is below 990 hPa (type W5). The largest SAT departures from normal are in western Canada and Alaska, but the area of positive anomalies also includes the eastern Bering Sea (Fig. 8p).

The C2 pattern (Figs. 9a–d) describes those cases when the Aleutian low is east of the critical longitude of 156°W, and the low-level northeasterly winds prevail in the Bering Sea. This type of circulation was observed, for example, during January 1983, and it offset the effect of the W5 type of circulation that occurred in December 1982 and February 1983. As a result, the 1982/83 El Niño event overall had little impact on the mean winter conditions in the Bering Sea (Niebauer 1988). During the other strong El Niño event of 1997/98, two winter months, December 1997 (normal) and February 1998 (cold) were classified as C2, which in combination with the C1 type of circulation in January 1998 resulted in a rather cold winter, particularly in terms of ice cover, which was the heaviest since the regime shift of 1976/77 (Fig. 3).

The Aleutian low in the C3 circulation pattern (Fig. 9e) is not as deep as in the W3 pattern (Fig. 8e). This difference, however, was not characteristic enough for CART to separate W3 and C3 based on the variable "central pressure." The Aleutian low in C3 is still stronger than normal, and both the SLP (not shown) and 700-hPa-height (Fig. 9g) anomalies in the central North Pacific are negative. This pattern resembles the second empirical orthogonal function (EOF) for January–March 700-hPa-height anomalies computed by Overland et al. (2002). Unlike W3, the increased cyclonic activity in the central North Pacific in the case of C3 does not lead to increased advection of warm Pacific air into the Bering Sea. The C3 pattern lacks high pressure anomalies over western Canada and Alaska, and the 700-hPa geostrophic wind is from the northeast over the Bering Sea where advection should have a cooling effect. The Siberian high is anomalously strong (Fig. 9g), which causes increased advection of cold Arctic air along its eastern periphery and cooling of the Bering Sea (Fig. 9h).

It is also interesting to compare the C4 (Figs. 9i–l) and W4 (Figs. 8i–l) patterns, which have many similar features, but are associated with opposite SAT anomalies in the Bering Sea. In both patterns the Aleutian low is split, and a high pressure cell of 700-hPa anomalies dominates the central North Pacific. At the sea level, the difference is that in the case of C4, the eastern SLP center (in the Gulf of Alaska) is stronger than the western one, whereas for W4 it is the opposite. The configuration of 700-hPa-height anomalies (Fig. 9k) suggests that it is the anomalously strong northwesterly winds from Siberia (instead of southwesterly winds in the case of W4) that causes below-normal temperatures in the Bering Sea (Fig. 9l).

The least frequent among the cold patterns is C5 (Figs. 9m–p). There were only six cold months associated with this pattern during the period of 1950–2002, and two months during the period of 1916–49. This type of atmospheric circulation is characterized by the strong southwesterly geostrophic winds over the eastern North Pacific (Fig. 9o) that bring warm Pacific air to western Canada and part of Alaska (Fig. 9p). In comparison to the W5 pattern (Fig. 8o), the center of negative 700-hPa-height anomalies in Fig. 9o is shifted farther north, and, hence, a greater portion of the Bering Sea is subject to anomalous flow from the north and cool SAT (Fig. 9p).

6. Interdecadal variability

Winter temperatures at St. Paul do not experience any significant systematic trend over the period of record (Fig. 10a). Variations on the interdecadal time scale, however, are rather substantial. It is interesting to compare these variations with changes in frequency of two major circulation types for the Bering Sea—W1 and C1. Although there is a general opposition between temporal variations in these two types, it is not always the case (Fig. 10b). Particularly interesting to consider is the climate shift of 1976/77 from severe winters of the early 1970s to very mild winters after the shift. By the mid-1970s, the frequency of the C1 type reached its maximum for the entire 1916–2002 period, and then dropped to its minimum by the early 1980s. In contrast, the increase in frequency of the W1 type (which reached its maximum only in the late 1980s) was more gradual and not in pace with the rapid warming after the climate shift. Likewise, a small peak in the frequency of this circulation type in the late 1930s was less than adequate to explain a significant warming in that period.

The warming in the early 1920s, late 1930s, and late 1970s appears to have much to do with cyclonic activity in the central North Pacific (south of 51°N). Because both the W3 and C3 types of circulation are characterized by an increased cyclonic activity in this region, it is interesting to examine changes in the combined frequency of these two types. Figure 10c shows frequency (number of months per winter season) of those situations when the Aleutian low had a single center located south of 51°N and west of 156°W (the leftmost branch of the tree in Fig. 4, before the last split into W3 and C3). These numbers were smoothed by a low-pass But-
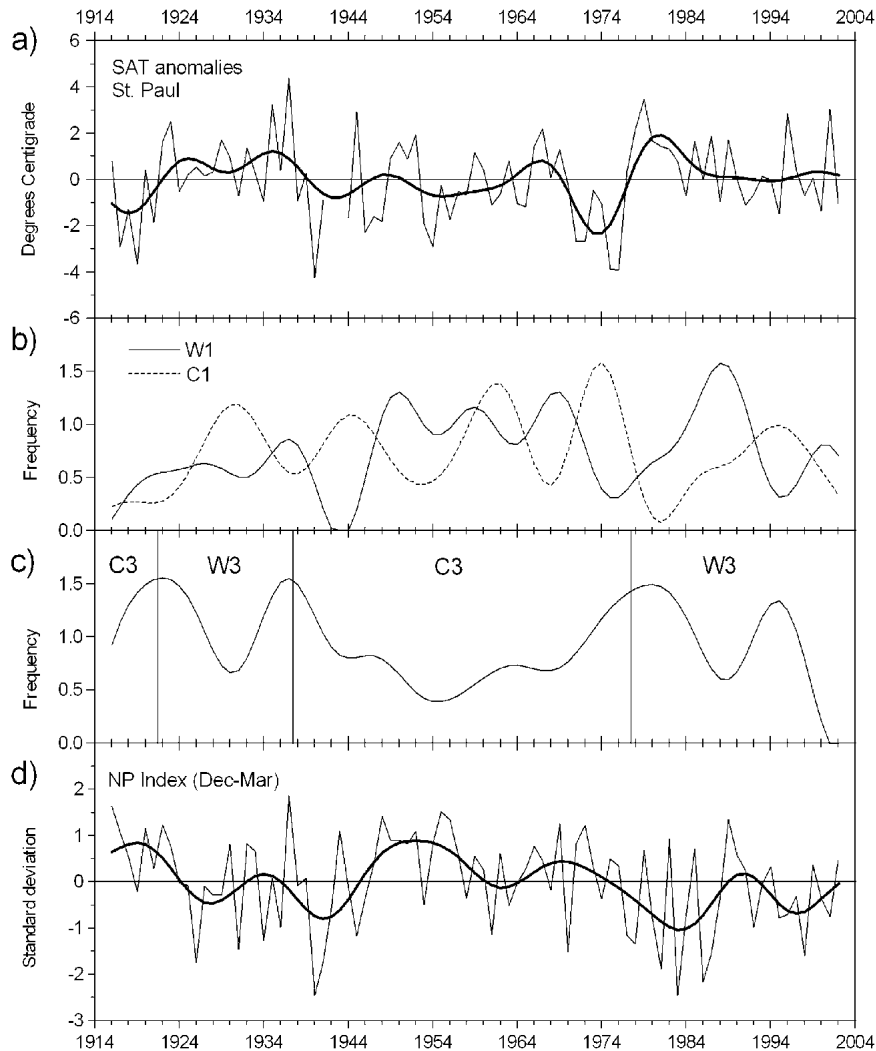
FIG. 10. (a) Normalized SAT anomalies at St. Paul (1916–49: SAT_{GISS}; 1950–2002: SAT_{PMEL}), mean winter values (thin line), and low-pass-filtered (Butterworth filter with the 10-yr cutoff period) values (bold line); (b) low-pass-filtered frequency (number/year) of the W1 and C1 circulation types; (c) same for the combined frequency of the W3–C3 types; and (d) mean winter (DJFM, thin line) and low-pass-filtered (bold line) values of the North Pacific index, 1916–2002. Vertical lines indicate the years of transition between W3 and C3 regimes.

terworth filter with the 10-yr cutoff period. First, it bears noting that the characteristic time scale of the combined W3/C3 variability is longer than that of the W1 and C1 types, despite the fact that all of the time series were passed through the same filter. Another interesting aspect is that the years of transition between the W3 and C3 periods coincide, or almost coincide, with three major peaks in the W3/C3 frequency.

The sequence of events around the turning points between the W3 and C3 regimes can be described as following. In the late 1910s, the frequency of C3 types started to increase. Atmospheric pressure in the central North Pacific, as depicted by the North Pacific (NP) index (Fig. 10d), was still well above normal. The high frequency of C3 types meant a tendency for cold in the

Bering Sea. In fact, the late 1910s were as cold as the early 1970s (Fig. 10a). Beginning about 1922, when the Aleutian low was centered south of 51°N, it translated into above-normal SAT anomalies in the Bering Sea. The shift around 1922 was not associated with a decrease in SLP; it dropped later, after 1925 (Fig. 10d), which marked the beginning of a positive phase of the PDO (Mantua et al. 1997). The increase in the frequency of W3 types in the late 1930s appeared to be a major factor contributed to the warming in the Bering Sea during this period. A shift from the W3 to C3 regimes occurred around 1937 and was accompanied by a rapid cooling in the Bering Sea (Fig. 10a). An increase in the frequency of C3 types became noticeable again in the early 1970s, when, staring with 1970, every winter

(except 1972) had at least 1 month of the C3 type. In the winter of 1976/77, a switch between the C3 and W3 regimes took place, this time simultaneously with a decrease in the NP index and a shift to a new, warm PDO phase.

The importance of the W3/C3 maximum in the mid-1990s is not clear. Three winters in a row—1995, 1996, and 1997—each had 2 months of the W3/C3 type, but with no clear switch from the W3 regime to the C3 regime. Beginning with the El Niño winter of 1997/98, no W3/C3 types were observed until at least the winter of 2001/02—the last winter considered here. This was a record long period (5 yr) with no W3/C3 types in a single month.

7. Summary and concluding remarks

This study examines a relationship between the Aleutian low and SAT anomalies in the eastern Bering Sea during winter (DJFM) months. Using the CART technique, 10 types of atmospheric circulation were classified—five of them were found to be associated with anomalously warm conditions in the Bering Sea, and five with anomalously cold conditions. It is important to emphasize that in doing this we used the absolute values of the Aleutian low characteristics (central pressure and geographical position), not their anomalies, thus, avoiding the dependency from the reference period, which often represents a problem in analyses of long time series. The classification tree obtained here turned out to be quite stable over time and performed well on both the model-development (1950–2002) and independent (1916–49) datasets. The analysis of the tree shows that Bering Sea temperatures are more sensitive to changes in the geographical position of the Aleutian low than in its central pressure.

Two types of atmospheric circulation were found to be of primary importance for the Bering Sea. The first type, W1, occurs when the Aleutian low deepens (relative to its climatological mean) and shifts west and north of its mean position in connection with an increased cyclonic activity in the western Bering Sea. These cyclones pump warm Pacific air into the eastern Bering Sea where SAT anomalies are, on average, 2°–4°C above normal. This type of atmospheric circulation accounts for 50% of all "warm" months and there were no "cold" months observed under these conditions. In other words, this type of atmospheric circulation has high classification purity.

The second type, C1, represents a split Aleutian low with one center in the northwestern Pacific (but south of 52°N) and the other in the Gulf of Alaska. A high pressure cell dominates in the Bering Sea. The advection of cold Arctic air along the eastern periphery of this cell causes the temperature in the eastern Bering Sea to drop 2°–4°C below normal, on average. This type accounts for 38% of all cold months, but there were two

misclassified warm months, so that the classification purity of this type is somewhat less than that for W1.

Secondary types, W2–W5 and C2–C5, describe a variety of other atmospheric patterns associated with warm and cold months in the Bering Sea. A comparison of these patterns shows that almost similar circulation anomalies can be associated with both below- and above-normal temperatures in the Bering Sea. On the other hand, seemingly opposite circulation anomalies can lead to the same SAT anomalies in the Bering Sea.

Temporal variability in frequency of the W1 and C1 types shows that while the two tend to be out of phase, it is not always the case, as during the climate shift around 1977. Similarly, there is no full spatial opposition in SLP anomalies between these patterns, which suggests the overall nonlinearity of the system.

The variability in a combined frequency of W3 and C3 types occurs on a longer, multidecadal time scale, compared with the decadal time-scale characteristic of the W1 and C1 types. It is important to emphasize that the separation of these two time scales was an unexpected product of this work, and not the result of a targeted filtering. It points to a principal difference between climatic processes in the North Pacific and Bering Sea that appear to operate on a different time scale. This difference is reflected in a different temperature response to the Aleutian low in these two regions. Thus, strengthening of the Aleutian low is almost invariably associated with a positive phase of the PDO with negative SST/SAT anomalies in the western and central North Pacific and positive anomalies along the North American coast (Mantua et al. 1997). For the Bering Sea, however, it may mean either positive or negative temperature anomalies, depending on the position of the Aleutian low. The same holds true for the weakening of the Aleutian low.

This paper presents the first portion of our research on the atmospheric circulation of the North Pacific and the weather of the Bering Sea. The next facet of this work will focus on how changes in the Aleutian low impact storm tracks, because it is ultimately the latter that largely control the tangible weather.

REFERENCES

Anderson, J. R., and J. R. Gyakum, 1989: A diagnostic study of Pacific basin circulation regimes as determined from extratropical cyclone tracks. *Mon. Wea. Rev.,* **117,** 2672–2686.

Beamish, R. J., C. E. Neville, and A. J. Cass, 1997: Production of Fraser River sockeye salmon (Oncorhynchus nerka) in relation to decadal-scale changes in the climate and the ocean. *Can. J. Fish. Aquat. Sci.,* **54,** 543–554.

Benson, A. J., and A. W. Trites, 2002: Ecological effects of regime

shifts in the Bering Sea and eastern North Pacific Ocean. *Fish Fish.,* **3,** 95–113.

Bjerknes, J., 1966: A possible response of the atmospheric Hadley circulation to equatorial anomalies of the ocean temperature. *Tellus,* **18,** 820–829.

——, 1969: Atmospheric teleconnections from the equatorial Pacific. *Mon. Wea. Rev.,* **97,** 163–172.

Breiman, L., J. H. Friedman, R. A. Olshen, and C. J. Stone, 1984: *Classification and Regression Trees.* Chapman and Hall, 358 pp.

Burrows, W. R., and R. A. Assel, 1992: Use of CART for diagnostic and prediction problems in the atmospheric sciences. *Proc. 12th Conf. on Probability and Statistics in Atmospheric Sciences,* Toronto, ON, Canada, Amer. Meteor. Soc., 161–166.

Fang, Z., and J. M. J. Wallace, 1994: Arctic sea ice variability on a time scale of weeks and its relation to atmospheric forcing. *J. Climate,* **7,** 1897–1914.

Hollowed, A. B., S. R. Hare, and W. S. Wooster, 2001: Pacific Basin climate variability and patterns of northeast Pacific marine fish production. *Progress in Oceanography,* Vol. 49, Pergamon, 257–282.

Hsu, H.-H., and J. M. Wallace, 1985: Vertical structure of wintertime teleconnection patterns. *J. Atmos. Sci.,* **42,** 1693–1710.

Hughes, J. P., D. P. Lettenmaier, and P. Guttorp, 1993: A stochastic approach for assessing the effect of changes in regional circulation patterns on local precipitation. *Water Resour. Res.,* **29,** 3303–3315.

Kalnay, E., and Coauthors, 1996: The NCEP/NCAR 40-Year Reanalysis Project. *Bull. Amer. Meteor. Soc.,* **77,** 437–471.

King, J. R., V. V. Ivanov, V. Kurashov, R. J. Beamish, and G. A. McFarlane, 1998: General circulation of the atmosphere over the North Pacific and its relationship to the Aleutian low. Department of Fisheries and Oceans, Science Branch—Pacific Region, Pacific Biological Station North Pacific Anadromons Fish Commission Doc. 318, 18 pp.

Luchin, V. A., I. P. Semiletov, and G. E. Weller, 2002: Changes in the Bering Sea region: Atmosphere–ice–water system in the second half of the twentieth century. *Progress in Oceanography,* Vol. 55, Pergamon, 23–44.

Mantua, N. J., S. R. Hare, Y. Zhang, J. M. Wallace, and R. C. Francis, 1997: A Pacific interdecadal climate oscillation with impacts on salmon production. *Bull. Amer. Meteor. Soc.,* **78,** 1069–1079.

McFarlane, G. A., J. R. King, and R. J. Beamish, 2000: Have there been recent changes in climate: Ask the fish. *Progress in Oceanography,* Vol. 47, Pergamon, 147–169.

Miller, A. J., D. R. Cayan, T. P. Barnett, N. E. Graham, and J. M. Oberhuber, 1994: The 1976–77 climate shift of the Pacific Ocean. *Oceanography,* **7,** 21–26.

Mock, C. J., P. J. Bartlein, and P. M. Anderson, 1998: Atmospheric circulation patterns and spatial climatic variations in Beringia. *Int. J. Climatol.,* **18,** 1085–1104.

Niebauer, H. J., 1983: Multi-year sea ice variability in the eastern Bering Sea: An update. *J. Geophys. Res.,* **88,** 2733–2742.

——, 1988: Effects of El Nino–Southern Oscillation and North Pacific weather patterns on interannual variability in the subarctic Bering Sea. *J. Geophys. Res.,* **93,** 5051–5068.

——, 1998: Variabillity in Bering Sea ice cover as affected by a regime shift in the Pacific in the period 1947–1996. *J. Geophys. Res.,* **103,** 27 717–27 737.

——, N. A. Bond, L. P. Yakunin, and V. V. Plotnikov, 1999: An update on the climatology and sea ice of the Bering Sea. *Dynamics of the Bering Sea,* T. R. Loughlin and K. Ohtani, Eds., University of Alaska Sea Grant, 29–60.

Overland, J. E., and C. H. Pease, 1982: Cyclone climatology of the Bering Sea and its relation to sea ice extent. *Mon. Wea. Rev.,* **110,** 5–13.

——, J. M. Adams, and N. A. Bond, 1999: Decadal variability of the Aleutian low and its relation to high-latitude circulation. *J. Climate,* **12,** 1542–1548.

——, N. A. Bond, and J. M. Adams, 2002: The relation of surface forcing of the Bering Sea to large-scale climate patterns. *Deep-Sea Res.,* **49B,** 5855–5868.

Renwick, J. A., and J. M. Wallace, 1996: Relationships between North Pacific wintertime blocking, El Niño, and the PNA pattern. *Mon. Wea. Rev.,* **124,** 2071–2076.

Rodionov, S. N., and R. A. Assel, 2000: Atmospheric teleconnection patterns and severity of winters in the Laurentian Great Lakes basin. *Atmos.–Ocean,* **38,** 601–635.

Rogers, J. C., 1981: The North Pacific Oscillation. *J. Climatol.,* **1,** 39–57.

Stabeno, P. J., N. A. Bond, N. B. Kachel, S. A. Salo, and J. D. Schumacher, 2001: On the temporal variability of the physical environment over the south-eastern Bering Sea. *Fish. Oceanogr.,* **10,** 81–98.

Trenberth, K. E., and D. A. Paolino, 1981: Characteristic patterns of variability of sea level pressure in the Northern Hemisphere. *Mon. Wea. Rev.,* **109,** 1169–1189.

——, and J. W. Hurrell, 1994: Decadal atmosphere–ocean variations in the Pacific. *Climate Dyn.,* **9,** 303–319.

Walker, G. T., and E. W. Bliss, 1932: World weather V. *Mem. Roy. Meteor. Soc.,* **4,** 53–84.

Wallace, J. M., and D. S. Gutzler, 1981: Teleconnections in the geopotential height field during the Northern Hemisphere. *Mon. Wea. Rev.,* **109,** 784–812.

Wooster, W. S., and A. B. Hollowed, 1995: Decadal-scale variations in the eastern subarctic Pacific: I. Winter ocean conditions. *Proc. Symp. on Climate Change and Northern Fish Populations,* Ottawa, ON, Canada, Canadian Special Publication of Fisheries and Aquatic Sciences 121, National Research Council of Canada, 81–85.

Wyllie-Echeverria, T., and W. S. Wooster, 1998: Year-to-year variations in Bering Sea ice cover and some consequences for fish distributions. *Fish. Oceanogr.,* **7,** 159–170.

Zorita, E., and H. von Storch, 1999: The analog method—A simple statistical downscaling technique: Comparison with more complicated methods. *J. Climate,* **12,** 2474–2489.

——, J. Hughes, and D. P. Lettemaier, 1995: Stochastic characterization of regional circulation patterns for climate model diagnosis and estimation of local precipitation. *J. Climate,* **8,** 1023–1042.